

1 **Seismic Anisotropy of the Victoria Land Region, Antarctica**

2

3

4 Salimbeni S.<sup>1</sup>, Pondrelli S.<sup>1</sup>, Danesi S.<sup>1</sup>, Morelli A.<sup>1</sup>

5

6

7

8

9

10 *<sup>1</sup> Istituto Nazionale di Geofisica e Vulcanologia, Sezione di Bologna, Via D. Creti 12,*  
11 *40128 Bologna, Italy*

12

13 Accepted date:            Received date            ; in original form date

14

15 **Short Title:** Seismic Anisotropy of the Victoria Land region, Antarctica

16

17 **Corresponding author:** Salimbeni S., Istituto Nazionale di Geofisica e Vulcanologia, Sez. di  
18 Bologna, Via D. Creti 12, 40128 Bologna, Italy; [salimbeni@bo.ingv.it](mailto:salimbeni@bo.ingv.it); Fax: +39 0514151499

19

20

21

## 22 SUMMARY

23

24 We present shear-wave splitting results obtained from the analysis of core refracted teleseismic  
25 phases recorded by permanent and temporary seismographic stations located in the Victoria Land  
26 region (Antarctica). We use an eigenvalue technique to isolate the rotated and shifted shear-wave  
27 particle motion, in order to determine the best splitting parameters. Average values show clearly  
28 that dominant fast axis direction is NE-SW oriented, in accordance with previous measurements  
29 obtained around this zone. Only two stations, OHG and STAR show different orientations, with  
30 N-S and NNW-SSE main directions. On the basis of the periodicity of single shear-wave  
31 splitting measurements with respect to back-azimuths of events under study, we infer the  
32 presence of lateral and vertical changes in the deep anisotropy direction. To test this hypothesis  
33 we model waveforms using a cross-convolution technique for the cases of one and two  
34 anisotropic layers. We obtain a significant improvement on the misfit in the double layer case for  
35 the two stations. For stations where a multi-layer structure does not fit, we investigate lateral  
36 anisotropy changes at depth through Fresnel zone computation. We find that anisotropy beneath  
37 the Transantarctic Mountains (TAM) is considerably different from that beneath the Ross Sea.  
38 This feature influences the measurement distribution for the two permanent stations TNV and  
39 VNDA. Our results show a dominant NE-SW direction over the entire region, but other  
40 anisotropy directions are present and maybe interpreted in the context of regional tectonics.

41

42 **Keywords:** Antarctica, Mantle Processes, Seismic Anisotropy, Shear-wave Splitting

43

## 43 INTRODUCTION

44

45 Splitting of shear-waves from teleseismic earthquakes is a powerful tool to investigate the  
46 structure of the upper mantle in different geodynamic environments. Since anisotropy may be a  
47 result of deformational events, shear-wave splitting studies permit investigation of the  
48 geodynamical processes, which have acted on the area of interest.

49

50 Shear-wave splitting is the seismological analogue of optical birefringence. When an S-wave  
51 passes through an anisotropic medium, it will be split into two quasi-S waves travelling with  
52 different velocities (Savage, 1999). The vibration direction of the faster phase and the difference  
53 in arrival time (delay time) between the two phases, are parameters recovered from this analysis.  
54 Teleseismic shear-wave splitting of core-refracted phases (e.g. SKS, SKKS) enables the study of  
55 the anisotropy located on the station-side of the epicenter-station path. Most of the anisotropy  
56 contribution originates in the upper mantle region where olivine is the most abundant mineral  
57 (Silver, 1996; Savage, 1999). Since olivine is highly anisotropic, its crystals develop a preferred  
58 orientation when a geodynamical process acts. In the simple shear case, Lattice Preferred  
59 Orientation (LPO) is generated by dislocation glide (Karato *et al.*, 2008) and [100]  
60 crystallographic-axis rotates parallel to the direction of the maximum shear (Savage, 1999) that  
61 also corresponds to the faster direction of S-wave vibration direction after splitting. Therefore the  
62 study of anisotropy can provide insights into deformational processes which have acted at a  
63 regional scale.

64

65 The harsh climatic conditions and the inaccessibility of the Antarctic region make it difficult to  
66 operate permanent or long-term seismic instrumentation. Few data are available, therefore any  
67 additions to the collective dataset are very important in understanding the tectonics of the  
68 Antarctic region. In recent years, several studies, which make use of seismic anisotropy, have  
69 been carried out, but the overall dataset remains sparse. The current study adds new data and  
70 interpretation which improves existing spatial coverage.

71 In East Antarctica, previous shear-wave splitting studies for the Dronning Maud Land area  
72 (Bayer *et al.*, 2007) suggested mainly NE-SW anisotropy direction, with some nearly N-S  
73 directions, that authors interpreted as due to crust-mantle coupling deformation. NE-SW is also  
74 the main direction for stations located in other inland areas (e.g. at South Pole; Muller, 2001),  
75 whereas shear-wave splitting measurements for coastal stations are generally oriented parallel to  
76 the coastline as observed for the Lambert Glacier region (Reading and Heintz, 2008). In West  
77 Antarctica, NE-SW continues to be the dominant direction beneath the Transantarctic Mountain  
78 (TAM) belt (Barklage *et al.*, 2009) and in the Victoria Land region (Pondrelli and Azzara, 1998;  
79 Pondrelli *et al.*, 2005). These measurements are interpreted to be related to the TAM uplift, while  
80 NW-SE and E-W directions, present sporadically around the Ross Sea, are interpreted as linked  
81 to extensional processes which have occurred in the past.

82

83 Some studies found also indications of possible two-layer anisotropic structure; Muller (2001)  
84 proposed the presence of a two anisotropic layers beneath the Scotia Plate and beneath the  
85 western stations of Dronning Maud Land justifying the anisotropy sampled in the upper layer as  
86 due to the signature of an Archaean frozen-in anisotropy while the origin of the lower layer

87 would go back to the Gondwana rifting stages. In the Lambert Glacier and Wilkes Land areas,  
88 Reading and Heintz (2008) admitted the possible presence of a two-layer structure for coastal  
89 stations even if the small amount of data didn't allow modelling the upper mantle anisotropy  
90 with the detail obtained by Heintz and Kennet (2006) for the adjacent Australian plate.

91

92 In the following, we describe the anisotropy measured for the Victoria Land region, West  
93 Antarctica. Using together data recorded at permanent stations VNDA and TNV and data from  
94 temporary stations sited around the David Glacier, we show the indications for the presence of  
95 different local domains of anisotropy, with a possible double-layer anisotropic system with  
96 lateral changes, a configuration more complex than that previously shown for this region. Here  
97 we provide an improved study of the regional seismic anisotropy distribution, we identify new  
98 heterogeneities and we describe a more detailed Victoria Land structure.

99

## 99 **GEOLOGICAL AND GEOPHYSICAL SETTINGS**

100

101 Antarctica is commonly divided into two main geological domains, East and West, with very  
102 different structural and geophysical characteristics (Figure 1). East Antarctica (EA) is classified  
103 as a Precambrian craton, the central part of the Palaeozoic Gondwana super-continent. West  
104 Antarctica (WA) is interpreted as the assembly of Meso-Cenozoic crustal blocks (Dalziel and  
105 Elliot, 1982) or micro-plates with metamorphic and volcanic terranes (Anderson, 1999). The  
106 Ross Sea and the West Antarctic Rift System (WARS) are part of West Antarctica and represent  
107 the extensional basins developed after Cretaceous and Cenozoic extensions (Behrendt, 1999).  
108 Evidence of active alkaline volcanism is present with Mount Erebus and Mount Melbourne  
109 volcanoes (Figure 1).

110 The Transantarctic Mountains (TAM) range separates the East from the West region of the  
111 continent. The TAM is a 3500 km long and 200 km wide chain composed, together with the  
112 Victoria Land region, of Cambrian and younger rocks. It is considered an intra-continental  
113 mountain belt with lack of evidence of compression. Its origin is attributed to an asymmetric  
114 uplift of the crust along the Ross embayment flank and subsequent denudation from Cretaceous  
115 to Cenozoic time (Fitzgerald, 1992, 1995; Studinger *et al.*, 2004). Fission track analyses  
116 (Fitzgerald, 1992) establish the beginning of the main uplift phase at about 50 Ma.

117 Most of the surface and deeper geological structures of the Victoria Land region can be ascribed  
118 to the Ross Orogeny. The Meso-Cenozoic evolution of the Ross Sea has seen two main phases of  
119 extension; from 105 to 55 Ma, characterized by E-SE extensional faulting, and from 55 to 32  
120 Ma, generating N-S and NNW-SSE tectonic depression. These extensional phases were followed

121 by right-lateral strike-slip tectonics from 32 Ma to the present.

122

123 The tectonic fabric of the crystalline basement also originated during the Ross Orogeny, but in  
124 early Palaeozoic times (500-480 Ma). The fabric is defined by steeply dipping metamorphic  
125 foliation, highly strained shear zones and fold axial trends, in a main NW-SE direction (Salvini  
126 and Storti, 1999). Surface structures in the Victoria Land region can be divided into 3 principal  
127 fault systems (Salvini and Storti, 1999). The first one is a NW-SE right-hand strike-slip fault  
128 system along which major glaciers stream; the second one is composed by N-S depression  
129 profiles interpreted as extensional or transtensional structures associated to Cenozoic, right-  
130 lateral shear; the third one includes NE-SW and NNE-SSW faults present in the Terra Nova Bay  
131 area, bordering the western shoulder of the Ross Sea, connected to the TAM uplift. Fault  
132 directions are parallel to the coastline and tend to rotate to N-S and NW-SE moving towards  
133 south.

134 Several different seismological methods provide structural information which highlights the  
135 dramatic discontinuity between East and West Antarctica.

136 Combining receiver function and phase velocity inversions, Lawrence *et al.* (2006b) derived  
137 crustal thickness in various parts of the study region. They show that beneath the Ross Sea the  
138 crust is 20 km thick (+- 2 km), and increases to 40 km (+- 2 km) beneath the TAM. A uniform 35  
139 km thick crustal layer characterizes the cratonic domain in East Antarctica. These values are also  
140 in agreement with several previous works (Bentley, 1991; Bannister *et al.*, 2003; ten Brink *et al.*,  
141 1997). The crustal structure of northern Victoria Land has been investigated also by Piana  
142 Agostinetti *et al.* (2004). Analysing receiver functions they found a 24 km crustal thickness in

143 the Robertson Bay area, with an increase to 31 km westwards of the Transantarctic Mountains  
144 (Oates Land). This would suggest that the crustal profile remains approximately stable moving  
145 southwards beneath coastal stations, while it changes laterally (at different longitudes). Beneath  
146 the stations located in the TAM chain, the authors find evidence of two Moho interfaces between  
147 26 and 48 km in depth.

148 Another seismological difference between East and West Antarctica concerns shear-wave  
149 velocities. The TAM divides a “fast” eastern upper mantle with velocities of 4.5 km/s (typical of  
150 a continental shield) from a “slower” western one where velocities decrease to 4.2 km/s (typical  
151 for active tectonics and volcanic regions). These values are in agreement also with those inferred  
152 from the study of regional surface wave velocities (Danesi and Morelli, 2001; Morelli and  
153 Danesi, 2004; Ritzwoller *et al.*, 2001). The transition between West and East occurs at 100 +/- 50  
154 km inland near the crest of the TAM (Lawrence *et al.*, 2006c). The same transition separates a  
155 colder eastern region from a warmer western one (Lawrence *et al.*, 2006a). The increment in  
156 mantle temperature is 200-400 °C (at 80-220 km depth), approximately corresponding to a  
157 reduction of 1% in density.

158

159 Previous shear-wave splitting measurements in the Victoria Land region and neighbouring areas  
160 are shown in Figure 2. Pondrelli *et al.* (2005) measured shear-wave splitting in the northern part  
161 of the study area (in purple in Figure 2). Only non-null splitting measurements are plotted on the  
162 map and, following the representation of the authors, any measurement is plotted at location  
163 corresponding to 150 km of piercing point depth. This procedure is used only with measurements

164 obtained from single event analysis and each measurement is plotted at the surface projection of  
165 the ray path at the depth of 150 km. This representation evidences any difference in anisotropy as  
166 a function of back-azimuth of studied events, to focus on the possible presence of lateral and  
167 vertical changes. The depth choice allows to interpret the total contribution of the anisotropy as  
168 located on the upper mantle (Savage, 1999). Near TNV station, measurements have NE-SW  
169 dominant fast velocity direction while the average delay time is estimated around 1.6 s. The  
170 authors linked this NE-SW direction to the presence of an old cratonic anisotropy and to mantle  
171 flows due to the growth of the TAM chain. The other directions (E-W and NW-SE) instead are  
172 interpreted as due to the extensional processes associated with the Western Rift system.

173

174 Results from the TAMSEIS Project (in yellow in Figure 2) are taken from Barklage *et al.* (2009).  
175 They obtained shear-wave splitting teleseismic measurements for 3 temporary arrays (yellow  
176 triangles) located principally on the southern part of the Victoria Land and extending inland  
177 toward East Antarctica. Splitting parameters are calculated using stacked-waveforms. At the  
178 intersections between E-W and N-S arrays, the fast direction is  $58^\circ$  and becomes more E-W  
179 towards the coast ( $67^\circ$ ). The delay time is about 1 sec. At the same intersection, comparing  
180 Rayleigh wave phase velocities from different azimuth values, Lawrence *et al.* (2006c) found a  
181 fast axis direction ranging between  $55^\circ$  and  $85^\circ$  with magnitude of 1.5-3.0% of anisotropy. In  
182 this area, Barklage *et al.* (2009) suggest anisotropy associated with an upper mantle flow related  
183 to Cenozoic Ross Sea extension or an edge-driven convection due to the sharp thermal change  
184 between West and East Antarctica. Towards the East Antarctica instead the measurements are  
185 distributed along a  $60^\circ$  ( $\pm 10^\circ$ ) direction that rotates to  $15^\circ$ - $20^\circ$  (becoming E-W) in two

186 highlands locations (Belgica and Vostok). The main distribution is described as being due to a  
187 relict tectonic fabric while the E-W measurements are interpreted as due to different extensional  
188 events maybe associated with older tectonic processes.

189

## 189 STATIONS AND DATA

190

191 We used data recorded by 11 seismic stations belonging to permanent and temporary networks in  
192 the Victoria Land region (Figure 2 and Table S1 on supplementary material). Permanent stations  
193 (cyan triangles in Figure 2) TNV and VNDA are located respectively on northern and southern  
194 margins of the study region. Both stations are equipped with 3-component broadband sensors  
195 (Streckeisen STS-1 and Geoteck KS-54000 Borehole respectively) with free access data  
196 availability managed by IRIS consortium (<http://www.iris.edu>). In the region also temporary  
197 stations have been installed. In the course of two expeditions within the Italian Scientific Project  
198 PNRA, during the 2003-2004 and 2005-2006 austral summers, we installed 9 broadband  
199 temporary seismic stations (blue circles in Figure 2) all equipped with Trillium T40 sensors and  
200 powered by solar panels and batteries. All the stations were located around the David Glacier  
201 running from the coast to the TAM on both sides of the glacier and cutting the chain  
202 perpendicularly, covering an area of 100x150 km<sup>2</sup>. One of these stations (STAR, cyan triangle)  
203 became permanent at the end of the first expedition and it continues operating.

204 We analysed records of teleseismic events occurring between 2003 and 2007, with Mw greater  
205 than 5.5 and epicentral distance between 85° and 120°. This distance range increases the  
206 likelihood of the presence and easy identification of the SKS arrival. These choices allow us to  
207 have a dataset for the temporary stations varying from a minimum of 2 months of data (e.g. site  
208 MORR) to a maximum of 5 years (site STAR). For both the permanent stations (VNDA and  
209 TNV) instead a two-year long dataset is complete.

210

## 210 SINGLE SHEAR-WAVE SPLITTING MEASUREMENTS

211

212 The fast axis orientation and the delay time between faster and slower phases are the two  
213 parameters provided by shear-wave splitting analysis. Most methods start assuming the  
214 anisotropic medium composed by one single layer with horizontal symmetry axis.

215

216 The fast velocity direction ( $\phi$ ) corresponds to the direction along which strain aligns the  
217 minerals; the delay time ( $dt$ ) allows to estimate the thickness of the anisotropic material. We  
218 retrieved these two parameters using the Silver and Chan (1991) method. This is based on a grid  
219 search over the possible splitting parameters that better remove the effects of anisotropy from the  
220 waveforms. In a general case, this can be done searching the most singular covariance matrix  
221 based on its eigenvalues  $\lambda_1$  and  $\lambda_2$ . A special case is when the initial wave polarization is  
222 known, as for SKS and SKKS phases, and when the signal-to-noise level is low; in this case the  
223 splitting parameters can be recovered minimizing the energy on the transverse component.

224

225 We used the SPLITLab environment (Wustefeld *et al.*, 2008), a Matlab graphical user interface  
226 (GUI) that enables the analysis of shear-wave splitting for large volumes of data and a quick  
227 quality check on the results. In addition, SPLITLab provides a method to calculate  
228 simultaneously shear-wave splitting parameters using the eigenvalue approach (EV),  
229 minimization of energy on the transverse component (SC, notation from Wustefeld *et al.*, 2008)  
230 and rotation-correlation technique (RC) (Fukao, 1984; Bowman and Ando, 1987) that removes  
231 the effect of splitting, maximizing the cross-correlation coefficient between radial (Q) and

232 transverse (T) components of the waveforms in the selected windows.

233

234 As the initial polarization of the wave is assumed to be radial, RC and SC methods are applicable  
235 to phases as SKS and SKKS; the EV method instead uses the back-azimuth as initial wave  
236 polarization and therefore it is applicable only for S phases. Synthetic tests on the RC and SC  
237 methods (Wustefeld and Bokelmann, 2007) demonstrate comparable results when the fast axis is  
238 far enough from the back-azimuth direction but show very different behaviours when the back-  
239 azimuth is close to the fast or slow direction (null directions). In this cases, the RC method  
240 deviates by  $45^\circ$  from the input fast axis, while the SC method yields scattered estimates around  
241 it. Therefore a comparison of results between these two methods distinguishes null  
242 measurements from the real splitting cases and allows us to assign a quality flag for any single  
243 measurement (Wustefeld and Bokelmann, 2007).

244

245 More specifically, we define the following parameters:

246

247  $\Delta\Phi = \Phi_{SC} - \Phi_{RC}$  and

248  $\rho = dt_{RC} / dt_{SC}$ .

249

250 and we pick “true” splitting measurements only if the following conditions are satisfied  
251 simultaneously:

252

253 1)  $\rho > 0.7$

254 2)  $|\Delta\Phi| < 22.5^\circ$

255 3) Signal-to-noise ratio (SNR) on the transverse component greater than 3

256

257 The measurement is flagged as "good" when  $\Delta\Phi < 8^\circ$  and  $0.8 < \rho < 1.1$ , "fair" when  $\Delta\Phi < 15^\circ$  and  
258  $0.7 < \rho < 1.2$  and "poor" in all other cases.

259

260 We consider null a measurement when an S-wave travelling through the medium has no  
261 splitting. This happens when the medium is isotropic or when the wave propagates along the so  
262 called null direction, that is the direction for which the initial wave polarization is parallel to the  
263 fast or slow axis (Savage, 1999). For SKS and SKKS cases, these directions coincide with the  
264 back-azimuth of the selected event. As suggested by Wustefeld and Bokelmann (2007), we can  
265 consider a measurement null when  $\Delta\Phi \sim n \cdot 45^\circ$  (with  $n$  an integer) and small  $\rho$ ; we consider "good  
266 nulls" when  $37^\circ < \Delta\Phi < 53^\circ$  and  $0 < \rho < 0.2$ , "fair nulls" when  $32^\circ < \Delta\Phi < 58^\circ$  and  $0 < \rho < 0.3$  and "poor  
267 nulls" in all other cases or when the SNR is lower than 3.

268

269 In the following we will consider only the SC measurements and we compare them with the  
270 results of the RC method for the quality assignment only.

271

272 Single station-event measurements obtained with the Silver and Chan (1991) method are shown  
273 on the map in Figure 3 and listed in Table S2 (splitting measurements) and Table S3 (null  
274 measurements) of the supplementary materials. For the sake of simplicity, in red we have plotted  
275 measurements flagged as "good" and in orange those flagged as "fair"; all measurements are

276 projected at a piercing point of 150 km depth to enhance any lateral variation in the anisotropy  
277 distribution beneath the station.

278 In total, we have 94 good and 44 fair splitting and 33 good and 37 fair null measurements. The  
279 distribution of the orientation of these measurements is very scattered (Figure 3). NNE-SSW  
280 seems to be the most frequent fast direction, but also NNW-SSE or N-S measurements are well  
281 visible. For some stations we have measurements perpendicular to each other as an expression of  
282 the possible presence of a complex anisotropic structure beneath the region. Nulls measurement  
283 distribution is in agreement with this single-splitting pattern.

284

285 The distribution of average values of splitting measurements, were calculated for single stations  
286 (Figure 4 and Table S4). When possible, the average values were calculated using good and fair  
287 measurements (dark blue segments) but in a few cases only fair measurements were used (cyan  
288 segments). In all cases nulls are excluded. Due to lack of results, caused by the few time of  
289 recordings and noisy data, in JYCE and MORR no average measurement is calculated. Most of  
290 the stations (TNV, VNDA, TRIO, HUGH) show a NE-SW direction and delay time values  
291 mostly compare well among them and in agreement with previous works. Station STAR has  
292 average fast axis with a NNW-SSE fast direction while in OHG the fast direction is N-S with a  
293 lower value of delay time. Stations with average anisotropy direction calculated with fair  
294 measurements (PHIL, PRST, and MDAN) show a uniform NNE-SSW direction, quite different  
295 with respect to surrounding stations.

296

297 The distribution of the measurements directions is comparable with previous works (Barklage *et*

298 *al.*, 2009; Pondrelli *et al.*, 2005). Our results however seem to estimate larger values of delay  
299 time; in fact, compared to the average values of 1 and 1.6 s calculated in the past, for most of our  
300 stations we also find values larger than 2 s and only at OHG we have a smaller delay time (1.5 s).  
301 This could be explained considering that we keep into account measurements until 4 s of delay  
302 time while the maximum value in Pondrelli *et al.* (2005) is 3 s providing smaller mean value.  
303 With respect to measurements in Barklage *et al.* (2009), instead, the difference is intrinsic in the  
304 calculation methods, given that in this last case the splitting parameters are calculated stacking  
305 waveforms for each station. In the next section, we will see that our mean values are comparable  
306 with those of this last work when we use a comparable method (as for example the cross-  
307 convolution technique).

## 308 VERTICAL CHANGES OF THE ANISOTROPY

309

310 The transverse energy minimization (SC) and rotation-correlation (RC) techniques described  
311 above allow the calculation of the splitting parameters based on two main assumptions  
312 concerning the structure of the anisotropic medium to analyse. The anisotropic medium is  
313 supposed to have one single anisotropic layer with anisotropy oriented along its horizontal axis.  
314 The splitting parameters provide a true value if the earth structure is well-drawn by the assumed  
315 model, while they give an "apparent" result if the real earth structure beneath the study site  
316 includes two or more anisotropic layers or the symmetry axis is not horizontal. A periodicity of  
317 the splitting parameters pattern with respect to the back-azimuth of the events usually indicates  
318 the presence of greater complexity (Savage, 1999; Menke and Levin, 2003).

319

320 In order to provide a possible interpretation to the variations that we obtain in our measurements,  
321 we studied the distribution of splitting parameters with respect to the back-azimuth of teleseismic  
322 earthquakes. Examples for VNDA, STAR and TNV are shown on Figure 5. Good (red crosses)  
323 and fair (blue crosses) splitting measurements and good (red circles) and fair (blue squares) null  
324 measures are displayed. The distribution of fast axis and delay time with respect to the back-  
325 azimuth seems to fit with different types of two-layer models (represented by green lines). The  
326 distribution of earthquake's back-azimuth is however discontinuous; for most events, phases  
327 under study come from NW or SE quadrants while the other back-azimuths are absent. Therefore  
328 a unique interpretation would be unreliable.

329

330 To test the vertical variation of anisotropy in a different way, we use a cross-convolution  
331 technique (Menke and Levin, 2003) to model all waveforms simultaneously and re-build the  
332 complex pattern of our measurements; we try to fit the data with an adequate two-layer model.  
333 The technique consists of two steps; first, splitting parameters for each event are calculated  
334 maximising the cross-correlation between horizontal rotated seismograms. Only events with a  
335 cross-correlation estimator value greater than 0.8 and modelled polarization within the error  
336 range of  $20^\circ$ , are picked for the following step. These criteria are so selective that only a small  
337 portion of data can be used for the inversion, generally about 8-9% of the complete dataset for  
338 each station. For this reason the inversion was carried out only for permanent stations TNV and  
339 VNDA and for those temporary stations having a wide range of day-recordings, namely STAR  
340 and OHG. The final solutions have been obtained using a minimum of 4 (OHG) and a maximum  
341 of 24 (VNDA) events.

342 In the second step we find the unique earth model structure that satisfies the entire group of  
343 observations with a grid-search inversion using a cross-convolution technique. Results are  
344 represented as an error surface plot as showed on Figure 6. The more complex model is chosen  
345 considering the distribution of the models on error surface plots and on the misfit reduction. In  
346 the example, therefore, for TNV the one-layer model is chosen as the best fitting whereas the  
347 two-layer model seems to be the best for OHG. Where the best solution is a double layer model,  
348 the final solution is selected by excluding those with a delay time greater than or equal to 3.0 sec  
349 and differences between two layer fast axis orientations ranging between  $80^\circ$  and  $100^\circ$ . This  
350 choice avoids near-normal fast polarization values whereby delay time in one layer cancels the  
351 delay time in the other (Menke and Levin, 2003).

352

353 The modelling results are displayed on the map in Figure 4 and listed in Table S5  
354 (supplementary material). Solutions for stations where a one layer earth structure fits the  
355 waveforms better than a double-layer model are shown with the violet lines oriented parallel to  
356 the fast axis and scaled accordingly to the delay time. Stations for which the double layer is the  
357 best model are represented with two colours: red for the lower and black for the upper layer. For  
358 each station the 10 solutions with lowest misfit are plotted.

359

360 Beneath VNDA and TNV stations, located respectively on the southern and northern margin of  
361 the region, a vertical variation of the anisotropy is absent. From the inversion we deduced that  
362 beneath TNV the dominant anisotropy shows a fast direction between  $41^\circ$  and  $44^\circ$  and delay  
363 time between 1.1 and 1.2 s. For VNDA the situation is similar, with a fast direction between  $36^\circ$   
364 and  $39^\circ$  and delay time ranging between 1.0 to 1.1 s. These values are consistent with the NE-  
365 SW alignment found for the averaged measurements and with previous papers.

366

367 Beneath STAR and OHG we infer that a two layer structure provides a best fit to the available  
368 data. These sites are located on structurally different places: STAR is sited along the coast, in an  
369 area where magma injection intruded along the Cenozoic N-S trending master faults (Rossetti *et*  
370 *al.*, 2000) while OHG is located inland, on the eastern shoulder of Prine Albert Mountains,  
371 characterized by pre-Cenozoic basements (Rossetti *et al.*, 2000). Nevertheless, the anisotropy  
372 shows similar patterns. Underneath STAR the fast axis for the lower layer varies from  $100^\circ$  to  
373  $150^\circ$  and delay time from 0.9 to 2.3 s; in the upper layer respective intervals are  $-10^\circ$  to  $40^\circ$  and

374 0.9 to 2.2 s. Beneath OHG, the fast axis direction for the lower layer varies in the range from  
375  $120^\circ$  to  $150^\circ$ , time delay from 1.2 to 1.6 s; for the upper layer fast axis directions are from  $-10^\circ$  to  
376  $20^\circ$  and time delay from 1.7 to 2.9 s. All these measurements are mutually consistent and close  
377 stations show similar fast-axis orientation for the upper layers (black lines).  
378

## 379 LATERAL CHANGES IN THE ANISOTROPY DIRECTION

380

381 Results obtained for the two permanent stations TNV and VNDA show scattering in the single  
382 event-station measurements, but absence of evidence for multi-layer structure. We hence  
383 investigate on the hypothesis of lateral changes of the anisotropy direction at depth as a possible  
384 interpretation of our measurements.

385

386 The computation of Fresnel zones, such as suggested by Alsina and Snieder (1995), helps to  
387 identify the presence of different patterns of anisotropy sampled from rays coming to the same  
388 station from different back-azimuths. Taking into account where the rays have a common path  
389 beneath the station it is possible to identify the depth interval at which this change occurs (Figure  
390 7).

391 The disturbance generated by an earthquake is influenced by physical properties of the earth in  
392 the vicinity of the geometrical ray path between source and receiver. This ray path can be  
393 approximated as a tube, the diameter of which is the Fresnel zone. The size of the Fresnel zone is  
394 a function of the wave frequency, and distance along the ray. For a steep-incidence phase, such  
395 as SKS or SKKS, it is approximately proportional to the depth beneath the receiver. The Fresnel  
396 zone at the depth  $h$ , can be calculated using (Pearce and Mittleman, 2002):

$$397 \quad R_f = \frac{1}{2} \sqrt{Tv h}$$

398 where  $R_f$  is the radius of the Fresnel zone expressed in km,  $T$  is the dominant period of the wave  
399 and  $v$  is the wave velocity. We choose  $T=10$  s as the dominant period of the wave, with the  
400 corresponding shear-wave velocity of S phase obtained from IASP91 model (3.75 km/s at 35 km,

401 4.476 km/s at 50 km, 4.49 km/s at 100 km, 4.45km/s at 150 km, 4.5 km/s at 200 km and 4.6 km/s  
402 at 250 km).

403 Examples for VNDA and TNV stations are shown in Figure 7; for each station we mapped the  
404 shear-wave splitting direction obtained studying two events coming from opposite back-  
405 azimuths. The two rays visibly sample different anisotropic patterns. If we take into account that  
406 these two rays share the same path beneath the station (see sketch included in Figure 7), the  
407 lateral change in the anisotropy should lay deeper than their conjunction point (Z depth on the  
408 inset). Indeed, below this depth the rays sample different regions of the upper mantle (blue  
409 circles on Figure 7) and above this depth the rays travel through the same anisotropic medium  
410 (yellow circles). The Fresnel zones are calculated for 35, 50, 100, 150, 200, 250 km of depth.  
411 Shared paths are represented by intersecting circles following opposite rays, vice versa paths  
412 along which rays are separated (thus, sampling different regions) are represented by non-crossing  
413 circles. The boundary between crossing and separated circles defines the depth at which the  
414 lateral variation occurs. We can deduce that for VNDA the lateral variation on the anisotropic  
415 properties occurs between 50 and 100 km of depth (last crossing and first separated circles  
416 respectively) while beneath TNV it occurs between 100 and 150 km of depth.

417

418 When we analyse rays coming from NW at both permanent stations, we obtain similar results,  
419 which indicate a dominant NE-SW anisotropy direction beneath the TAM. This is the most  
420 frequently measured direction for the region with no dependency on the recovery method.

421 On the contrary, rays coming from east seem to sample different anisotropic structures at the two  
422 sites - WNW-ESE for TNV and NW-SE for VNDA. These observations indicate two distinct

423 anisotropic characters in the TAM and the Ross Sea Embayment.

424

## 425 **DISCUSSION**

426

427 Figure 8 summarizes all our shear-wave splitting results (in colour) in the Victoria Land zone;  
428 for comparison we add measurements obtained by previous studies (in grey). The figure  
429 indicates the presence of different domains of anisotropy between margins and central part of the  
430 Victoria Land region.

431 At station TNV (northern region) we have a general agreement between different measurements.  
432 The NE-SW trend found by Pondrelli *et al.* (2005) and lately confirmed by Barklage *et al.* (2009)  
433 is in agreement with both our average of single measurements (blue stick) and our group  
434 inversion model (violet stick). Our last analysis suggests that the scattering in single  
435 measurements should not be ascribed to a vertical change in the anisotropy direction, at least at  
436 lithosphere-asthenosphere structure scale. The Fresnel zone computation shows that a lateral  
437 variation in anisotropic character at depth beneath TNV explains the splitting directions moving  
438 away from the dominant NE-SW.

439 In the southern region we have a similar situation. Our results for VNDA station are consistent  
440 and also agree with the splitting directions obtained for the temporary TAMSEIS network (in  
441 gray). The NE-SW direction is generally confirmed for stations moving towards the north.  
442 Again, the group inversion using our data excludes a vertical change in anisotropy directions  
443 beneath VNDA (at least at the scale we can investigate), while our Fresnel zone analysis  
444 supports the possibility of a lateral change at depth. This allows us to explain the single  
445 measurements trending away from the main NE-SW direction.

446 Some estimates for the thickness of the anisotropic layer in the area can be inferred from delay

447 time values of the grouped inversions. In both North and South Victoria Land, delay times range  
448 between 1.0 to 1.2 s. Given that Lawrence *et al.* (2006c) estimate 1 s delay time for a 150 km  
449 thick anisotropic medium, with 3% anisotropy, we infer that the thickness of the anisotropic  
450 layer should vary between 150 and 180 km.

451 From the calculation of the Fresnel zone, we can affirm that the anisotropic material should lay  
452 at a depth larger than 50-100 km (smaller values obtained respectively for VNDA and TNV),  
453 therefore the anisotropy thickness become in general greater than 200 km in depth. Since the  
454 lithosphere thickness beneath the Ross embayment was calculated in 250 km (Morelli and  
455 Danesi, 2004), anisotropy would be partially located in the lower lithosphere, with a possible  
456 contribution to the asthenospheric mantle.

457

458 The central part of the region has different features. The first difference is the direction of  
459 average fast axis measurements in OHG and STAR, which are N-S and NNW-SSE respectively.  
460 The mean directions calculated using only fair measurements (light blue stick on Figure 8)  
461 follow the same pattern.

462 Group inversion here gives a two-layer anisotropic model with NW-SE direction for the lower  
463 layer and N-S for the upper one. Since OHG is located on thick crust (about 35 km; Lawrence *et*  
464 *al.*, 2006c) and STAR on thinner crust (about 20 km), and considering that the anisotropy  
465 direction shows the same pattern, it is reasonable to expect that the anisotropy distribution is  
466 independent from the shallower structure, excluding (or limiting) a possible crustal contribution.  
467 Delay time values vary between 1.2-1.6 s and 0.9-2.3 s in the lower layers and between 1.7-2.9  
468 and 0.9-2.2 s in upper ones for OHG and STAR respectively, providing estimates for anisotropy

469 thickness of 435-675 km beneath OHG and 270-675 km beneath STAR. Considering that the  
470 lithosphere thickness is approximately 250 km, we infer an asthenospheric contribution.

471

472 From these results it appears that a narrow zone (approximately 100-150 km) separates a  
473 dominant NE-SW anisotropy of the northern and southern areas from the double layer structure  
474 inferred for stations closer to the David Glacier. Dominant directions for upper and lower layers  
475 are N-S and NW-SE respectively. The first orientation is in agreement with results found at some  
476 stations of the TAMSEIS array (gray lines on Figure 8) while the second direction matches with  
477 some single measurements close to station TNV (gray lines on Figure 8; Pondrelli *et al.*, 2005).  
478 TRIO and HUGH, temporary stations located in the central part of the study region, have a NE-  
479 SW mean value. On these sites however we could not apply group inversion or the Fresnel zone  
480 technique for lack of usable data.

481

482 Our measurements of anisotropy can be easily related to the tectonic features in the area, which  
483 indicate that crust and sub-continental mantle deform coherently (Vertically Coherent  
484 Deformation, VCD, as defined by Silver, 1996). The basic idea is that when more than one  
485 deformational event occurs, the effect of the younger is recorded on the hotter and deeper layer,  
486 while the oldest event remains recorded in the shallower and colder layer. With this concept in  
487 mind, we interpret the double layer anisotropic structure: the N-S direction of shallow anisotropy  
488 would be related to the deformation occurred during the second phase of extension (55-32 Ma),  
489 and the lower layer anisotropy would be related to the last transtensional event, that is still going  
490 on (32 Ma to the Present). In this context the NE-SW anisotropy can be interpreted as frozen-in

491 anisotropy relative to older geological events as inferred by several authors (Pondrelli *et al.*,  
492 2005; Barklage *et al.*, 2009), overprinted locally by more recent tectonic events. This hypothesis  
493 would also agree with possible lateral variations at depth. In fact, the contribution from western  
494 paths is in agreement with the NE-SW frozen-in anisotropy that would be beneath the TAM  
495 chain. More recent tectonic events have been taking place mainly in the Ross Sea, beneath which  
496 we sample WNW-ESE to N-S anisotropy directions.

497

498 Our measurements could also indicate an absolute plate motion (APM) contribution. The APM  
499 for the Antarctic plate on the Victoria Land region is 18° from N (green arrow on Figure 8; Gripp  
500 and Gordon, 2002) that is quite similar to the lower layer anisotropy direction. We therefore  
501 could deduce that the frozen-in anisotropy existing in the upper layer is linked to the two  
502 extensional phases of the Ross Orogeny and the APM contribution is constrained to exist in the  
503 lower layers. This hypothesis has been already investigated by Kendall *et al.* (2002) studying  
504 seismic anisotropy in continental environments as the Canadian shield. However, the low  
505 velocity of the Antarctic plate (1.3-1.6 mm/yr) does not produce necessarily the strain needed to  
506 generate this amount of anisotropy. Therefore, in agreement with Barklage *et al.* (2009), we  
507 suggest that this mechanism is not likely to be significant in the region that has been investigated  
508 in this study.

## 509 **CONCLUSIONS**

510

511 Shear-wave splitting measured in the Victoria Land region indicates that the NE-SW anisotropic  
512 direction is the most frequent orientation of anisotropy for stations located on northern and  
513 southern domains of the study region, in agreement with previous measurements. Here we add  
514 some new data supporting the presence of a lateral variation at depth, represented by a mainly  
515 NE-SW anisotropy direction beneath the TAM and some indications of a WNW-ESE to NW-SE  
516 anisotropy beneath the Ross Sea. For stations located around the David Glacier the distribution  
517 of single measurements is more scattered and the grouped inversion is consistent with the  
518 presence of a double anisotropic layer for the central area of the Victoria Land. The two  
519 dominant directions are N-S and NNW-SSE for the upper and lower layer respectively, in  
520 agreement with the direction of most of the tectonic structures in the area, presumably generated  
521 during the Ross Orogeny deformational phases.

522 This work has provided improved insights into the regional seismic anisotropy pattern, including  
523 newly identified heterogeneities and a more detailed picture of the structure of Victoria Land.  
524 Continued improvements to the database in the course of new field campaigns will allow further  
525 refinement of these results.

526

## 527 **ACKNOWLEDGMENTS**

528 We are very grateful to the referees, Dr A.M. Reading and Prof J. Trampert, for their  
529 constructive comments, which contributed to improve the manuscript. This work is supported by  
530 Programma Nazionale di Ricerche in Antartide (PNRA). All figures have been produced using

531 the GMT package (Wessel and Smith, 1991; Wessel and Smith, 1998).

532

## REFERENCES

- Alsina, D. and Snieder, R., 1995. Small-Scale Sublithospheric Continental Mantle Deformation - Constraints from Sks Splitting Observations, *Geophys J Int*, 123, 431-448.
- Anderson, J.B., 1999. *Antarctic Marine Geology*, edn, Vol., pp. Pages, Cambridge University Press, Cambridge.
- Bannister, S., Yu, J., Leitner, B. and Kennett, B.L.N., 2003. Variations in crustal structure across the transition from West to East Antarctica, Southern Victoria Land, *Geophys J Int*, 155, 870-884.
- Barklage, M., Wiens, D.A., Nyblade, A. and Anandakrishnan, S., 2009. Upper mantle seismic anisotropy of South Victoria Land and the Ross Sea coast, Antarctica from SKS and SKKS splitting analysis, *Geophys J Int*, 178, 729-741.
- Bayer, B., Muller, C., Eaton, D.W. and Jokat, W., 2007. Seismic anisotropy beneath Dronning Maud Land, Antarctica, revealed by shear wave splitting, *Geophys J Int*, 171, 339-351.
- Behrendt, J.C., 1999. Crustal and lithospheric structure of the West Antarctic Rift System from geophysical investigations — a review, *Global and Planetary Change*, 23, 25-44.
- Bentley, C.R., 1991. Configuration and structure of the subglacial crust. in *The Geology of Antarctica*, pp. 335-364, ed. Tingey, R. J. Oxford University Press, New York.
- Bowman, J.R. and Ando, M., 1987. Shear-wave splitting in the upper-mantle wedge above the Tonga subduction zone, *Geophysical Journal of the Royal Astronomical Society*, 88, 25-41.
- Dalziel, I.W.D. and Elliot, D.H., 1982. West Antarctica: Problem child of Gondwanaland, *Tectonics*, 1, 3-19.
- Danesi, S. and Morelli, A., 2001. Structure of the upper mantle under the Antarctic Plate from surface wave tomography, *Geophysical Research Letters*, 28, 4395-4398.
- Fitzgerald, P.G., 1992. The Transantarctic Mountains of Southern Victoria Land - the Application of Apatite Fission-Track Analysis to a Rift Shoulder Uplift, *Tectonics*, 11,

634-662.

- Fitzgerald, P.G., 1995. Cretaceous and Cenozoic exhumation of the Transantarctic Mountains: Evidence from the Kukri Hills of southern Victoria Land compared to fission track data from gneiss at DSDP site 270, *paper presented at Seventh International Symposium on Antarctic Earth Sciences, Terra Antarctica., Siena, Italy.*
- Fukao, Y., 1984. Evidence from Core-Reflected Shear-Waves for Anisotropy in the Earth's Mantle, *Nature*, 309, 695-698.
- Gripp, A.E. and Gordon, R.G., 2002. Young tracks of hotspots and current plate velocities, *Geophys J Int*, 150, 321-361.
- Heintz, M. and Kennet, L. N., 2006, The apparently isotropic Australian upper mantle, *Geophysical Research Letters*, 33, L15319, doi:10.1029/2006GL026401
- Karato, S., Jung, H., Katayama, I. and Skemer, P., 2008. Geodynamic significance of seismic anisotropy of the upper mantle: New insights from laboratory studies, *Annual Review of Earth and Planetary Sciences*, 36, 59-95.
- Kendall, J.M., Sol, S., Thomson, C.J., White, D.J., Asudeh, I., Snell, C.S. and Sutherland, F.H., 2002. Seismic heterogeneity and anisotropy in the western Superior Province, Canada; insights into the evolution of an Archaean craton. *in The early Earth; physical, chemical and biological development*, pp. 27-44, eds. Fowler, C. M. R., Ebinger, C. J. and Hawkesworth, C. J. Geological Society Special Publications, London, United Kingdom (GBR).
- Lawrence, J.F., Wiens, D.A., Nyblade, A.A., Anandkrishnan, S., Shore, P.J. and Voigt, D., 2006a. Upper mantle thermal variations beneath the Transantarctic Mountains inferred from teleseismic S-wave attenuation, *Geophysical Research Letters*, 33, -.
- Lawrence, J.F., Wiens, D.A., Nyblade, A.A., Anandkrishnan, S., Shore, P.J. and Voigt, D., 2006b. Crust and upper mantle structure of the Transantarctic Mountains and surrounding regions from receiver functions, surface waves, and gravity: Implications for uplift models, *Geochemistry Geophysics Geosystems*, 7, -.
- Lawrence, J.F., Wiens, D.A., Nyblade, A.A., Anandkrishnan, S., Shore, P.J. and Voigt, D., 2006c. Rayleigh wave phase velocity analysis of the Ross Sea, Transantarctic Mountains, and East Antarctica from a temporary seismograph array, *J Geophys Res-Sol Ea*, 111, -.
- Lythe, M.B., Vaughan, D.G. and Consortium, B., 2001. BEDMAP: A new ice thickness and

- subglacial topographic model of Antarctica, *J Geophys Res-Sol Ea*, 106, 11335-11351.
- Menke, W. and Levin, V., 2003. The cross-convolution method for interpreting SKS splitting observations, with application to one and two-layer anisotropic earth models, *Geophys J Int*, 154, 379-392.
- Morelli, A. and Danesi, S., 2004. Seismological imaging of the Antarctic continental lithosphere: a review, *Global and Planetary Change*, 42, 155-165.
- Muller, C., 2001. Upper mantle seismic anisotropy beneath Antarctica and the Scotia Sea region, *Geophys J Int*, 147, 105-122.
- Pearce, J. and Mittleman, D., 2002. Defining the Fresnel zone for broadband radiation, *Physical Review E*, 66, -.
- Piana Agostinetti, N., Amato, A., Cattaneo, M. and Di Bona, M., 2004. Crustal Structure of Northern Victoria Land from Receiver Function Analysis, *Terra Antarctica*, 11, 5-14.
- Pondrelli, S. and Azzara, R., 1998. Upper mantle anisotropy in Victoria Land (Antarctica), *Pure and Applied Geophysics*, 151, 433-442.
- Pondrelli, S., Margheriti, L. and Danesi, S., 2005. Seismic Anisotropy beneath Northern Victoria Land from SKS splitting Analysis. in *Antarctica: Contributions to global earth sciences*, pp. 153-160, eds. Futterer, D. K., Damaske, D., Kleinschmidt, G., Miller, H. and Tessensohn, F. Springer-Verlag, Berlin Heidelberg, New York.
- Reading, A.M. and Heintz, M., 2008. Seismic anisotropy of East Antarctica from shear-wave splitting: Spatially varying contributions from lithospheric structural fabric and mantle flow?, *Earth and Planetary Science Letters*, 268, 433-443.
- Ritzwoller, M.H., Shapiro, N.M., Levshin, A.L. and Leahy G.M., 2001. Crustal and upper mantle structure beneath Antarctica and surrounding oceans, *J. Geophys. Res.*, 106, 645-670.
- Rossetti, F., Storti F. and Salvini F., 2000. Cenozoic noncoaxial transtension along the western shoulder of the Ross Sea, Antarctica, and the emplacement of McMurdo dyke arrays, *Terra Nova* 12, 60-66.
- Salvini, F. and Storti, F., 1999. Cenozoic tectonic lineaments of the Terra Nova Bay region, Ross Embayment, Antarctica, *Global and Planetary Change*, 23, 129-144.

- Savage, M.K., 1999. Seismic anisotropy and mantle deformation: What have we learned from shear wave splitting?, *Reviews of Geophysics*, 37, 65-106.
- Silver, P.G., 1996. Seismic anisotropy beneath the continents: Probing the depths of geology, *Annual Review of Earth and Planetary Sciences*, 24, 385-&.
- Silver, P.G. and Chan, W.W., 1991. Shear-Wave Splitting and Subcontinental Mantle Deformation, *J Geophys Res-Sol Ea*, 96, 16429-16454.
- Studinger, M., Bell, R.E., Buck, W.R., Karner, G.D. and Blankenship, D.D., 2004. Sub-ice geology inland of the Transantarctic Mountains in light of new aerogeophysical data, *Earth and Planetary Science Letters*, 220, 391-408.
- ten Brink, U.S., Hackney, R.I., Bannister, S., Stern, T.A. and Makovsky, Y., 1997. Uplift of the Transantarctic Mountains and the bedrock beneath the East Antarctic ice sheet, *J. Geophys. Res.*, 102, 27,603–627,621.
- Wessel, P. and Smith, W.H.F., 1991. Free software helps map and display data, *EOS Trans. AGU*, 72, 441.
- Wessel, P. and Smith, W.H.F., 1998. New, improved version of generic mapping tools released, *EOS Trans. AGU*, 79, 579.
- Wustefeld, A. and Bokelmann, G., 2007. Null detection in shear-wave splitting measurements, *B Seismol Soc Am*, 97, 1204-1211.
- Wustefeld, A., Bokelmann, G., Zaroli, C. and Barruol, G., 2008. SplitLab: A shear-wave splitting environment in Matlab, *Comput Geosci-Uk*, 34, 515-528.

## FIGURE CAPTIONS

Figure 1: Map showing the elevation of the bedrock (Lythe *et al.*, 2001) in Antarctica and main structural and seismic regions. The zoomed map corresponds to the Victoria Land region.

Figure 2: Map showing broadband seismic stations operating in the Victoria Land region; cyan triangles are permanent stations (TNV, VNDA and STAR), blue circles are temporary stations. Yellow triangles represent the TAMSEIS project stations. In the same map previous shear-wave splitting measurements are shown; lines are oriented parallel to the fast axis with lengths proportional to delay time. Purple lines are results from Pondrelli *et al.* (2005) plotted for 150 km deep piercing points; yellow lines are results from Barklage *et al.* (2009) plotted at the surface.

Figure 3: Single splitting (map on the left) and null (map on the right) measurements obtained using the method of Silver and Chan (1991). In both maps good (red) and fair (orange) measurements are plotted using a piercing point of 150 km. Splitting measurements are plotted with line-segment oriented parallel to the fast axis with lengths proportional to delay time; null measurements are plotted with two cross-line oriented parallel to the back-azimuth and perpendicular to it. Blue circles and cyan triangles show locations (see Figure 2 for colour legend).

Figure 4: Average measurements (dark blue and cyan) and results of the inversion (violet and

red-black lines) calculated for each station. Average measurements: results in blue are calculated using good and fair measurements while those in cyan are obtained with only fair measurements. Grouped Inversion: for each station the 10 best solutions, with lowest misfit, are plotted. Violet lines represent one-layer best fitting model measures. Red and black lines respectively indicate lower and upper measures for two-layer best fitting models.

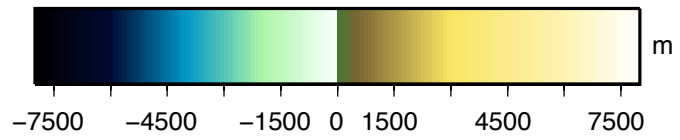
Figure 5: Examples of back-azimuth dependence of the splitting parameters for VNDA, STAR and TNV stations. Each panel contains good (red crosses) and fair (blue crosses) split measurements and good (red circle) and fair (blue square) nulls measurements. Poor results are excluded. Green lines on upper and medium panels correspond to the theoretical distribution of two-layer model with splitting parameters described above each figure. The distribution of single measurements is showed on lower plots.

Figure 6: Examples of error surface plots calculated in the grouped inversion for TNV and OHG stations in one (a and c) and two layers (b and d) cases. a,c) The white star indicates the minimum misfit error model. b,d) In white all regions where errors are greater than the one layer estimator; coloured areas correspond to regions where errors are smaller for the two-layer case. The two blue crossing-lines correspond to the one layer model solution. Green star is the lowest error misfit model.

Figure 7: Examples of Fresnel zones analysis for TNV and VNDA. Two events with opposite back-azimuth and different splitting parameters are analysed. Different size on the circles

corresponds respectively to 35, 50, 100, 150, 200, 250 km of depth of the Fresnel zone. In red we show the splitting measurements plotted at 35 km of depth. All intersecting circles in yellow represent the depth ( $Z$  on the inset) above which rays sampled the same anisotropy; in blue, separated circles define the depth below which rays sampled mediums with different anisotropic properties.

Figure 8: Summary map of shear-wave splitting results. Mean values of the single shear-wave splitting, calculated using good and fair split measurements, are in dark blue; mean values calculated with only fair measurements are in light blue; results from group inversion where the best model is the single one (10 better solutions) are in violet; red and black are 10 better solutions for lower and upper layer respectively. Previous results of Pondrelli *et al.* (2005) and Barklage *et al.* (2009) are plotted in grey. The big green arrow indicates the absolute plate motion of the Antarctica plate (Gripp and Gordon, 2002). Crustal thickness is taken from Lawrence *et al.* (2006b).



Topography

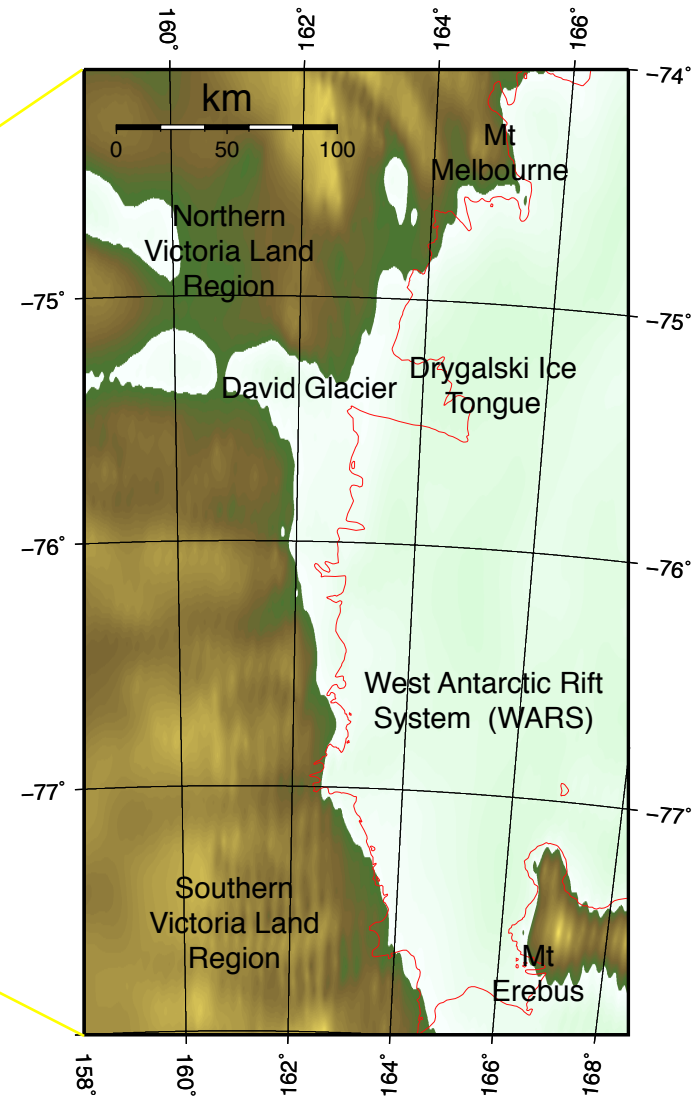
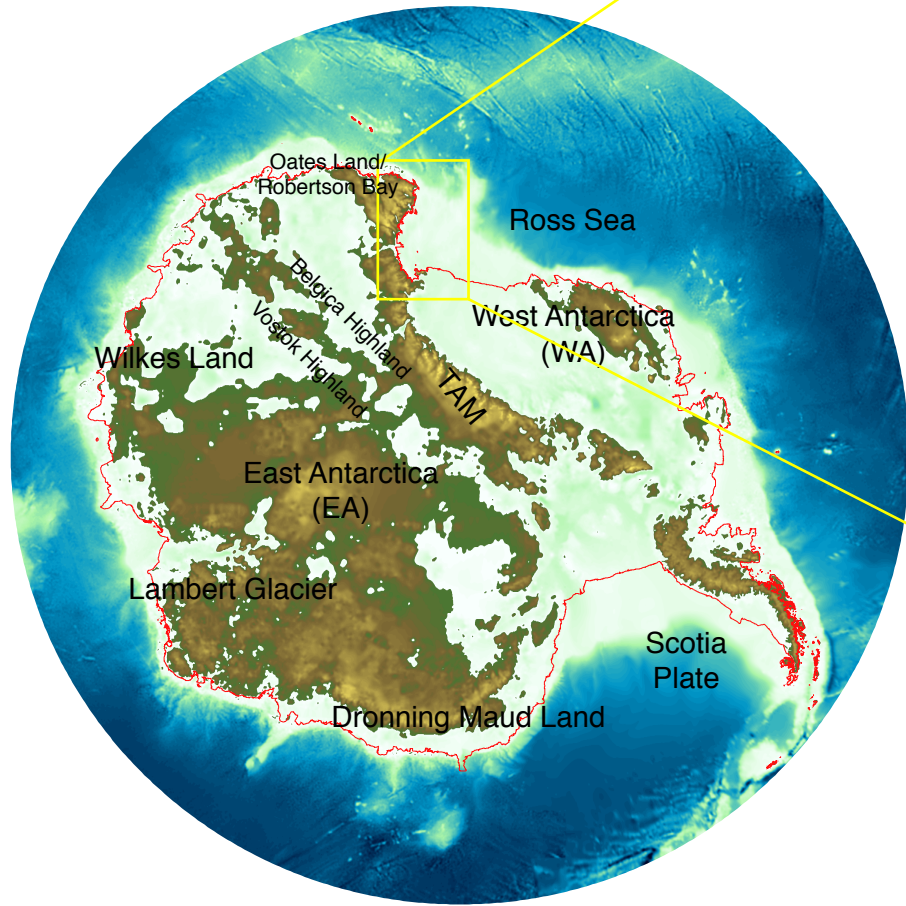


Figure 1

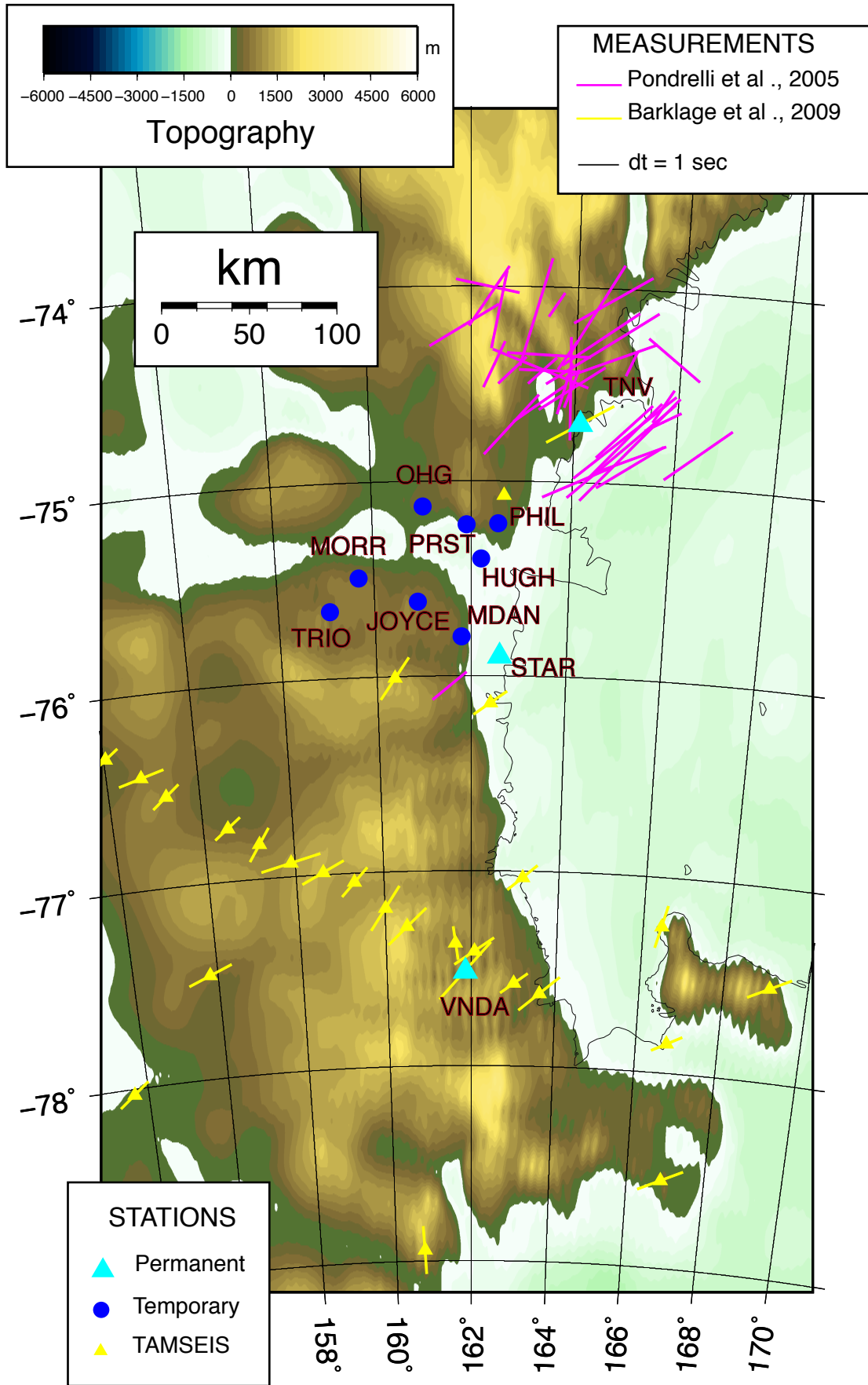


Figure 2

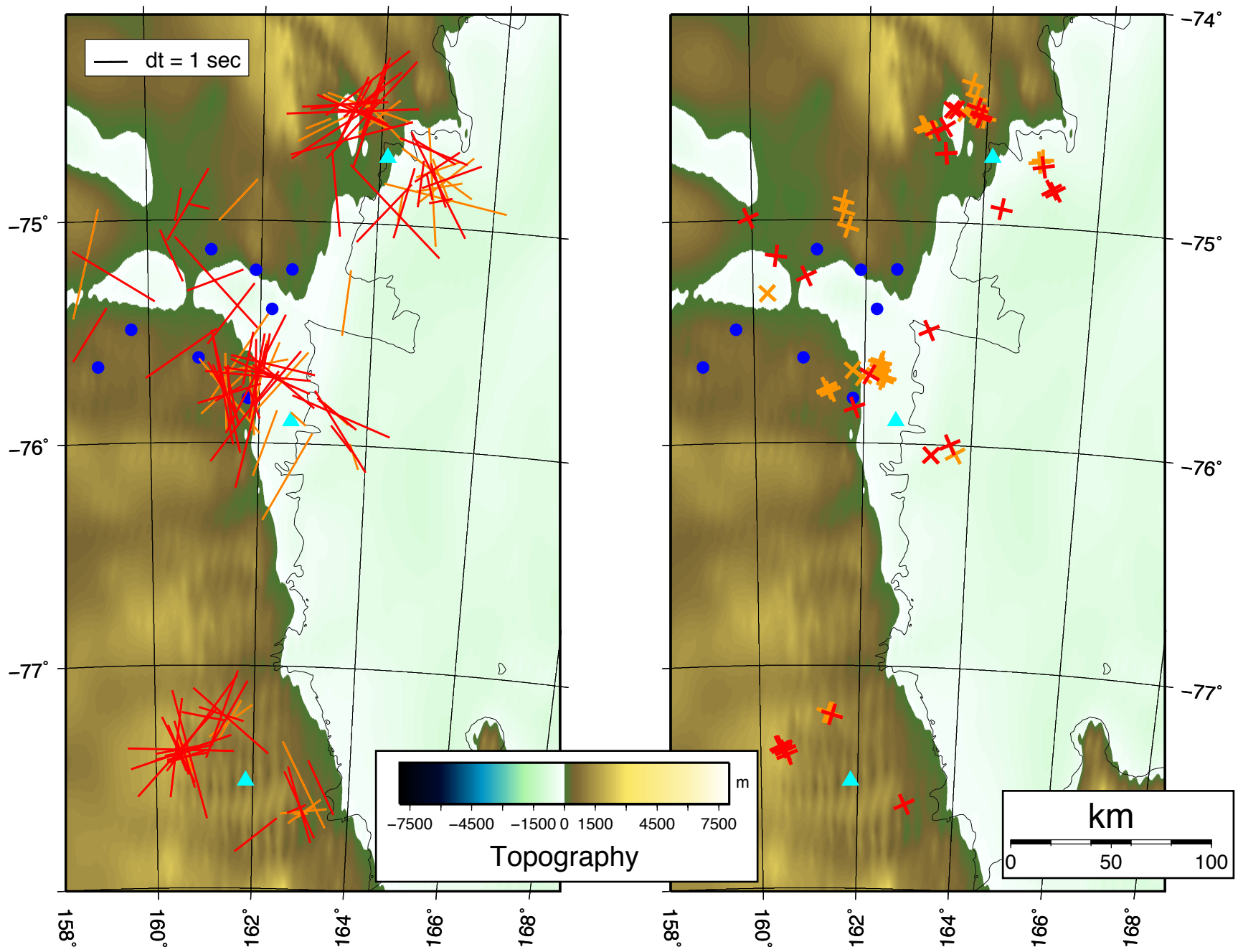
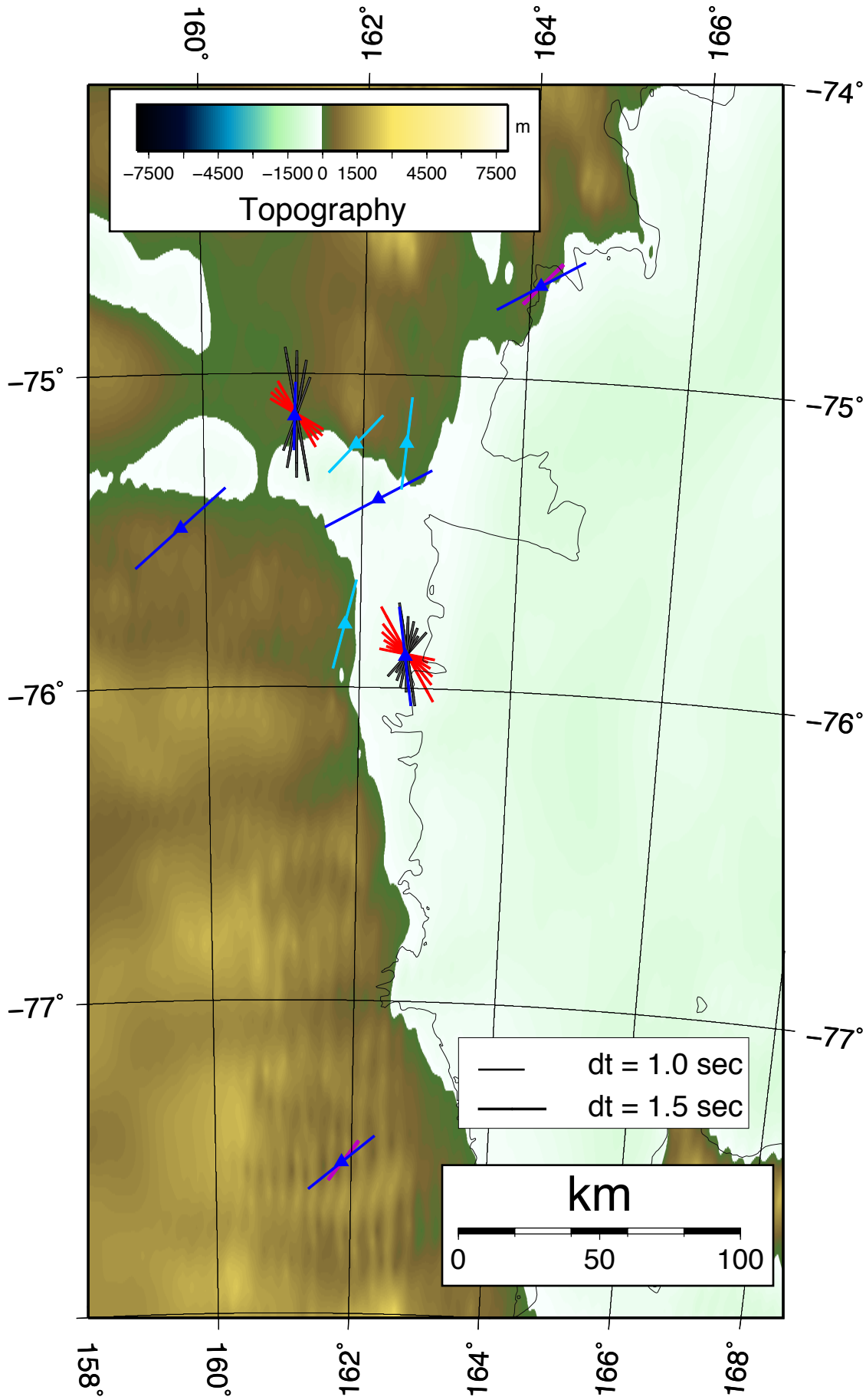


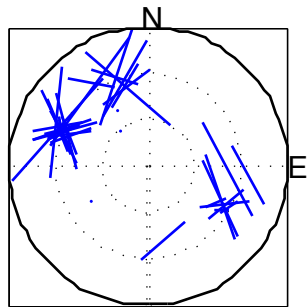
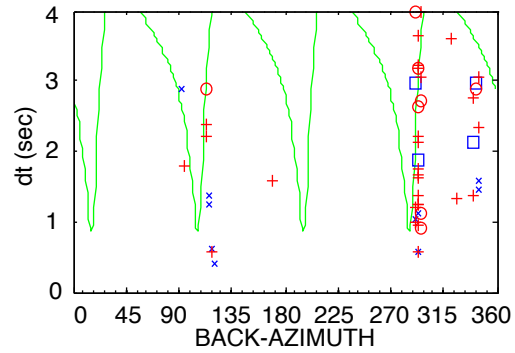
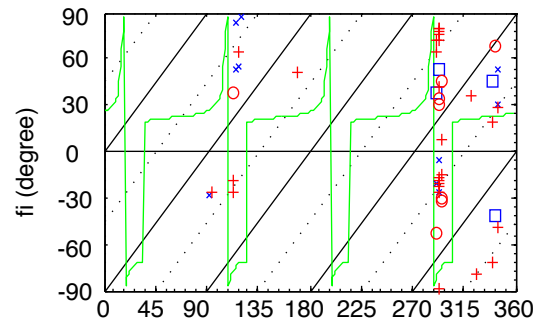
Figure 3

Figure 4



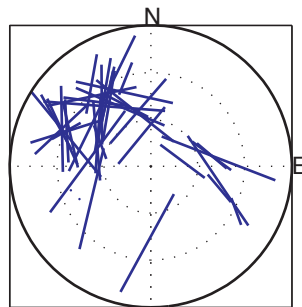
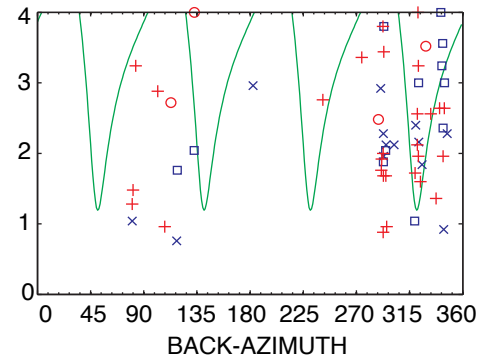
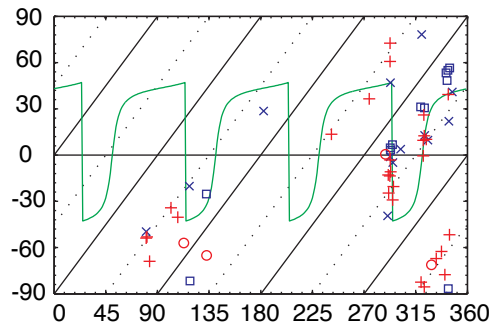
# VNDA

Upper Layer: 34.0, 1.6 s  
Lower Layer: 11.0, 2.5 s



# STAR

Upper Layer: 22.0, 1.5 s  
Lower Layer: 55.0, 3.1 s



# TNV

Upper Layer: 42.0, 1.3 s  
Lower Layer: 5.0, 1.9 s

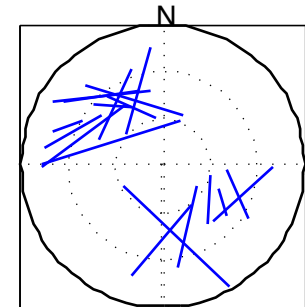
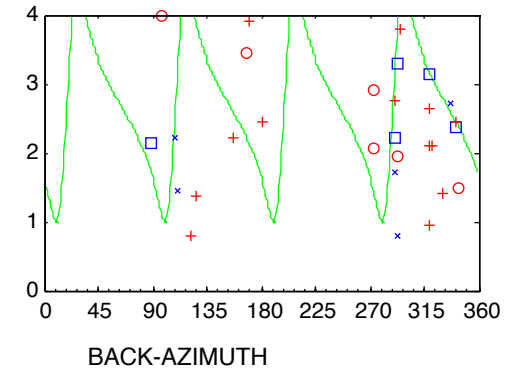
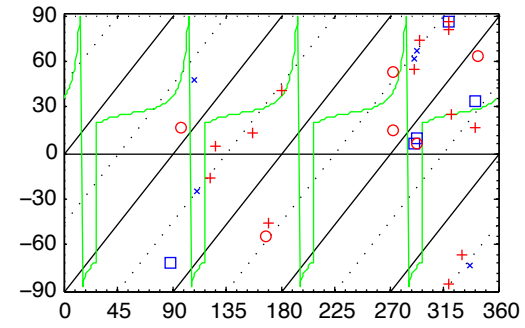
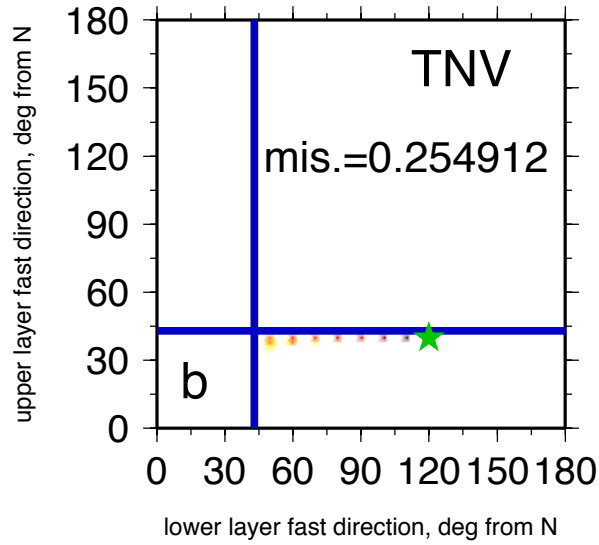
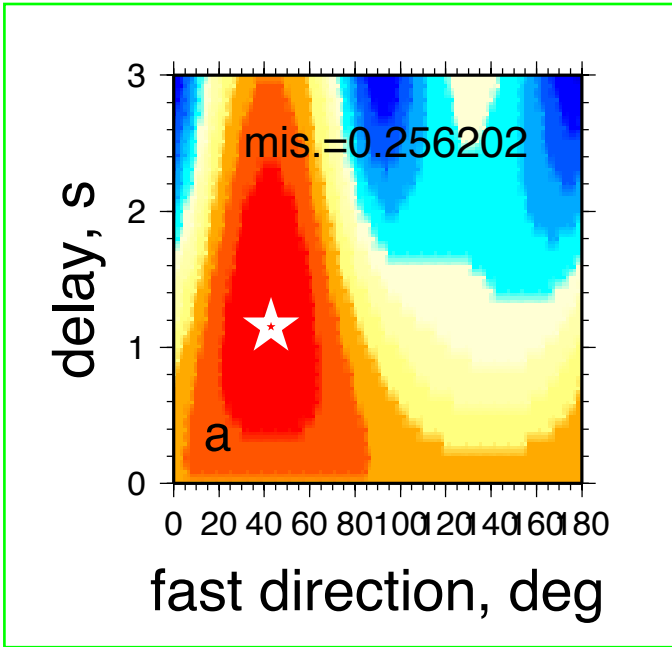
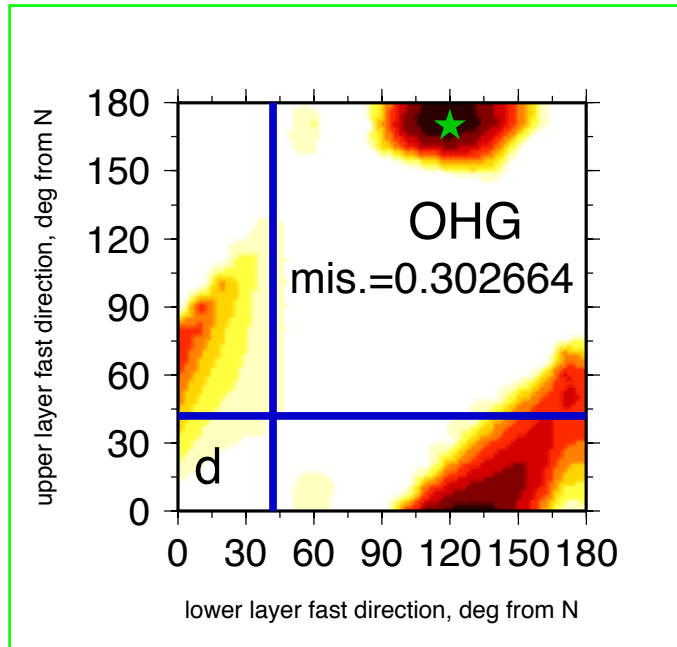
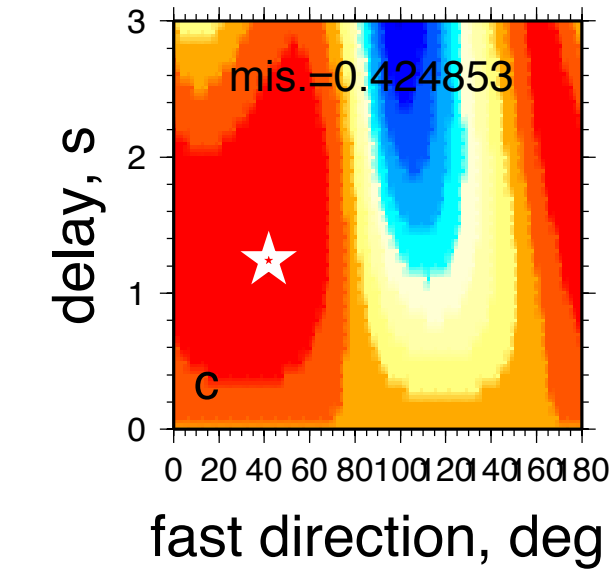


Figure 5



One layer best solution



Two layers best solution

FIGURE 6

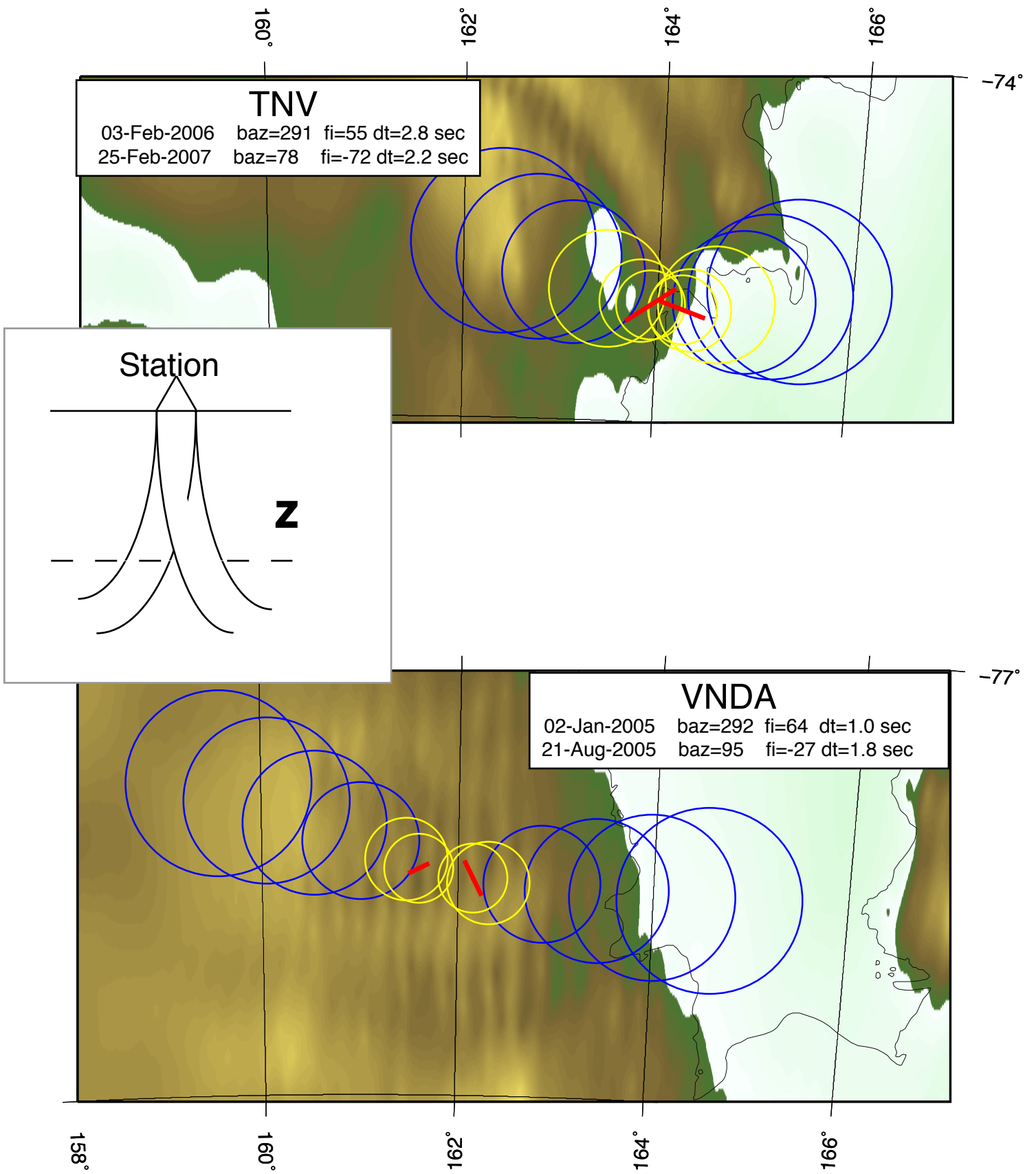


Figure 7

Figure 8

